Caving 2026 – A van As, D Cumming-Potvin & J Wesseloo (eds)
© 2026 Australian Centre for Geomechanics, Perth, ISBN 978-1-7636842-3-2
doi:10.36487/ACG_repo/2645_73

Geotechnical characterisation of Hugo North Lift 1, Oyu Tolgoi

Lawrence Rwodzi [a,*], Josef Ekkerd [b], Michael Taylor [b], Ankhbayar Batsaikhan [b], Andrea Russo [c], Catalina Ramírez [c], Esteban Hormazábal [c], Joled Nur [c]

[a] *Oyu Tolgoi, Rio Tinto, Mongolia*

[b] *Oyu Tolgoi, Rio Tinto, Australia*

[c] *SRK Consulting, Chile*

Abstract

Most major block cave operations in the world are hosted in porphyry orebodies, which pose significant geotechnical characterisation challenges due to their heterogenous and hydrothermally altered nature. The Hugo North Lift 1 block cave at Oyu Tolgoi is a large-footprint, deep cave hosted within a structurally complex porphyry system subjected to high stresses and exhibiting moderate to low strength rock mass conditions.

A comprehensive geotechnical block model covering the multiple production blocks at Oyu Tolgoi was developed over several years. Geotechnical units were defined using lithology, alteration, weak veinlet density and fault models, supplemented by drillhole composites. Fundamental rock mass characterisation parameters obtained from drillcore logging and underground tunnel mapping were estimated using statistical and geostatistical methods to populate the geotechnical block model. Extensive intact rock strength testing was also undertaken to inform the Hoek–Brown rock strength parameters adopted into the block model, and a dedicated methodology was developed to capture fault strength properties.

The resulting characterisation workflow and integrated block model have directly supported improved inputs into footprint stability assessments, fragmentation predictions, caveability and subsidence assessments, and have reduced geotechnical uncertainty in Hugo North Lift 1 design and sequencing.

This paper presents the characterisation methodology, resulting geotechnical insights for this complex porphyry orebody, and highlights key lessons learnt.

Keywords: *Oyu Tolgoi, geotechnical characterisation, geotechnical units, porphyry orebody, intact rock properties, fault strength properties*

1 Introduction

Hugo North Lift 1 (HNL1) at Oyu Tolgoi is one of the largest and deepest block cave mines currently in production. Located in the South Gobi Desert of Mongolia approximately 550 km south of Ulaanbaatar, the Hugo North deposit is part of a world-class porphyry copper-gold system. The block cave footprint extends over 2,000 m along strike and 280–500 m across. It comprises four mining blocks, namely Panel 0 (P0), Panel 1 (P1), Panel 2N (P2N) and Panel 2S (P2S), at a depth of approximately 1,300 m below surface, with 1,488 drawpoints planned across the full footprint (Figure 1).

The porphyry setting at Hugo North creates a geotechnical environment of exceptional complexity (Figure 2 and 3). The orebody is characterised by multiple intrusive phases overprinted by intense and spatially variable hydrothermal alteration (Figure 4). The orebody plunges to the north, bringing the deeper southern part of the orebody to a higher elevation. The principal mineralised lithologies – quartz monzodiorite (QMD), augite basalt (VA) and ignimbrite (IGN) – are overlain by the late- to post-mineralisation intrusive phase

* Corresponding author: Email address: Lawrence.Rwodzi@riotinto.com

biotite granodiorite (BiGd), which forms a dyke system along the western and central portions of the deposit. Heterogeneity is further increased by weak veinlet stockworks and lithological contact zones, together with a complex network of major fault structures that transect the deposit (Figures 2–4).

These challenges are compounded by high in situ stresses at 1,300 m depth. Together, these factors make geotechnical characterisation at Hugo North fundamentally more demanding than simpler, massive or weakly foliated rock mass environments.

A geotechnical characterisation program was progressively executed over 4 years (2019–2022), phased with the drilling campaigns for each production block. The resulting geotechnical block model integrates all characterisation data to support caveability assessments, footprint stability analyses, fragmentation predictions, subsidence modelling and detailed mine sequencing decisions. This paper describes the end-to-end methodology and presents key results under four themes: geotechnical unit definition and rock mass classification; intact rock strength characterisation; fault and discontinuity characterisation; and 3D geotechnical block model development and structural integration.

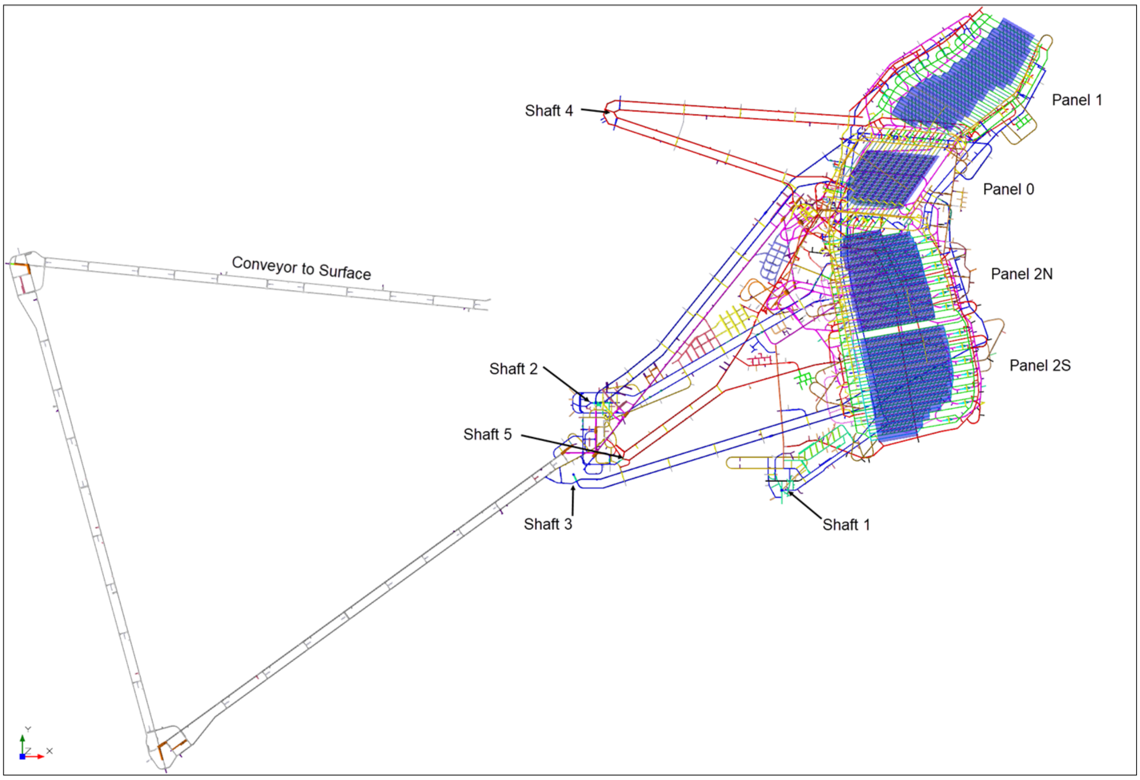

Figure 1 Plan view of all panels at Hugo North

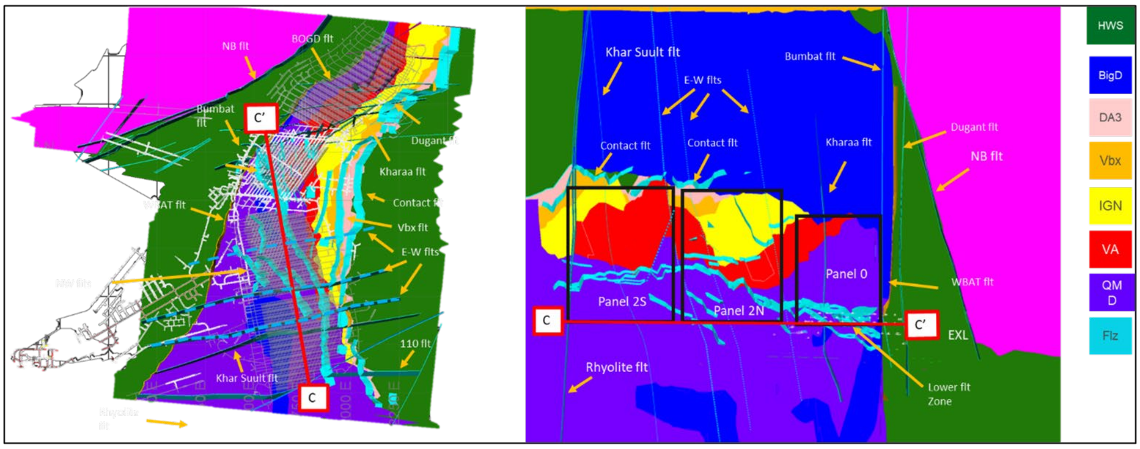

Figure 2 Lithology and structural model: P0, P2N and P2S

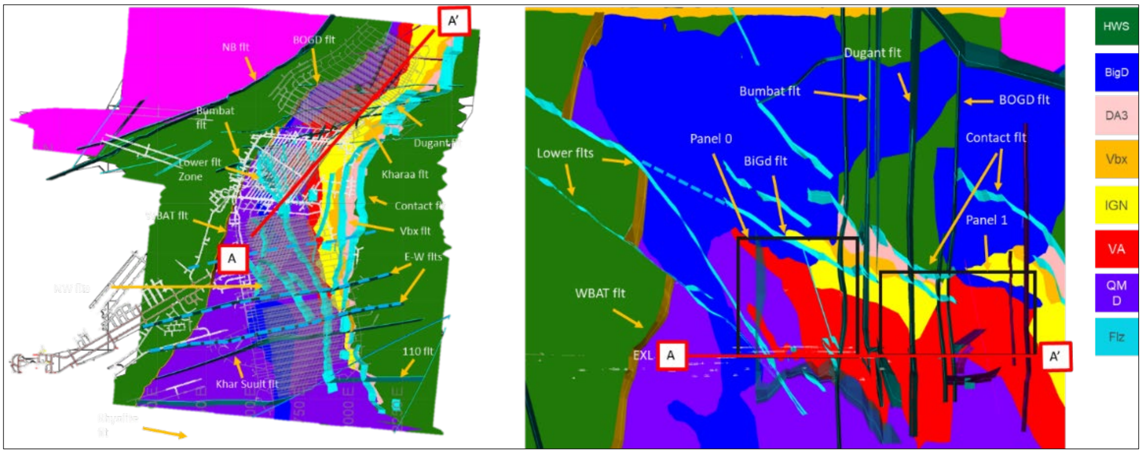

Figure 3 **Lithology and structural model: P0 and P1**

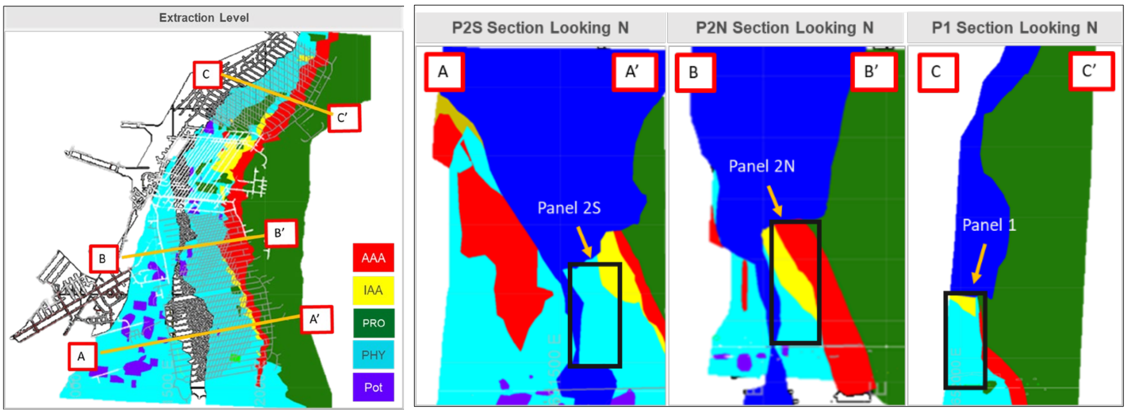

Figure 4 **HNL1 alteration model**

2 Geotechnical domaining

2.1 Definition of geotechnical units

Given the lithological, alteration and structural complexity of the Hugo North porphyry system, a bespoke basic geotechnical unit (BGU) framework was developed. A total of 36 geotechnical units were defined based on a hierarchical combination of:

- primary lithology (e.g. BiGd, QMD, VA, IGN, etc.; refer to Figure 2 and 3)
- hydrothermal alteration type (potassic, phyllic, propylitic, intermediate or advanced argillic, unaltered; refer to Figure 4)
- weak veinlet density – defined as the summed thickness per metre of veinlets with infill Mohs hardness <5.0 (a threshold of 15 weak veinlets per metre was applied to split the two main geotechnical units (BiGd and QMD) into low- and high-density sub-units after Russo et al. 2022)
- lithological contact zones, where contrasting mechanical properties generate structural heterogeneity
- fault zones (FZ1 and FZ2), characterised as rock mass units with their own classification parameters.

Figures 5 and 6 provide a plan view and section view of the HNL1 geotechnical domains. The wide distribution of geotechnical domains reflects the rock mass variability and justifies the extensive drilling and intact rock testing undertaken.

In addition to lithological variability, hydrothermal alteration is widely recognised to influence rock mass strength in porphyry deposits, as it modifies mineralogy, texture and mechanical properties of the host rock.

The same was observed at Hugo North. Figure 7 shows a general increase in intact rock strength from advanced argillic (AAA) through intermediate argillic (IAA) to phyllic (PHY) and potassic (PTS) alteration in the mining blocks. Relative to phyllic (low veinlet density), intact rock strength (σci) is approximately 42% lower in AAA and 22% lower in IAA.

Within the same lithology and alteration, the stockwork of veinlets with soft infill (<Mohs hardness <5) reduce σci over and above the impact that alteration type alone would suggest. This is consistent with findings by Brzovic & Villaescusa (2007) and Turichshev & Hadjigeorgiou (2016), who demonstrated in veined rock from El Teniente that peak strength is strongly governed by vein mineralogy and thickness, with failure predominantly occurring along weaker veinlets at low confinement. Day et al. (2019) similarly showed that conventional geological strength index (GSI) does not accurately capture rock mass strength in veined rock masses. They proposed a composite GSI (CGSI) methodology that explicitly incorporates intra-block structures such as hydrothermal veinlets and stockwork. This provides independent methodological support for subdomaining the dominant lithology and alteration by weak veinlet density to generate meaningful geotechnical domains rather than artificially averaging highly variable data. The Russo et al. 2022 methodology for quantifying weak veinlet density was adopted at Oyu Tolgoi. Following calibration of σci data, a threshold of 15 weak veinlets per metre was applied to subdivide the dominant units (BiGd and QMD) into low and high weak veinlet density domains. Within phyllic-altered QMD, an approximately 10% reduction in σci is observed between low and high weak veinlet density (Figure 7).

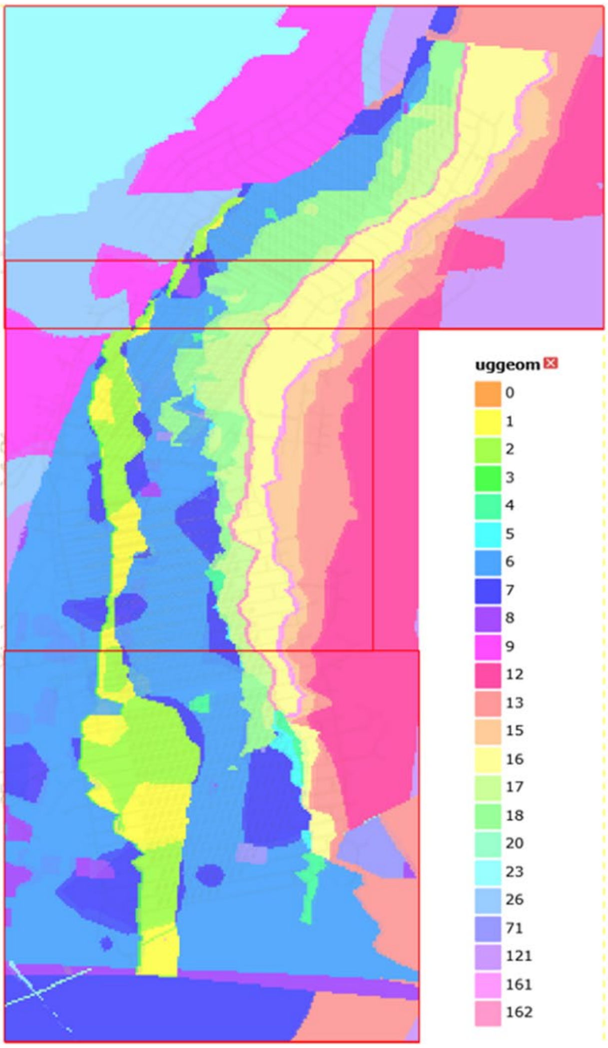

Block Model	Geotechnical Domains			
UGGEOM	GU	Lithology	Alteration	Weak Vein Density
0	BGU00	Cret_Clay	UALT	-
1	BGU01a	BiGd	UALT	Low
2	BGU01b	BiGd	UALT	High
3	BGU01c	BiGd-QMD contact	-	-
4	BGU04	QMD	AAA	-
5	BGU05	QMD	IAA	-
6	BGU06	QMD	PHY	Low
7	BGU07	QMD	PHY	High
71	BGU07A	QMD	PRO	-
8	BGU08	QMD	PTS	-
9	BGU09	BasL (CS3)	PRO+UALT	-
11	BGU11	Bat	PRO+UALT	-
12	BGU12	L	META+PRO	-
121	BGU12A	L	UALT	-
13	BGU13	Sst-Slt (Da3)	UALT	-
131	BGU13A	Vsst	UALT	-
14	BGU14	DacL	UALT	-
141	BGU14A	Dac	UALT+AAA	-
15	BGU15	Vbx	UALT	-
16	BGU16	IGN	AAA+IAA+PHY+PRO	-
161	BGU16A	Contact VBX-IGN	-	-
162	BGU16B	Contact Va-IGN	-	-
17	BGU17	Va	AAA + IAA	-
18	BGU18	Va	PRO+PTS+PHY	-
20	BGU20	RHY	UALT	-
21	BGU21	Ba	UALT	-
	BGU21a	Ba	PHY	-
	BGU21b	Ba	POT	-
22	BGU22	Cong	PHY	-
23	BGU23	HbBiGd	UALT	-
24	BGU24	xBiGd	UALT	-
	BGU25A	Qv90	AAA	-
	BGU25B	Qv90	PHY	-
26	BGU26A	And IGN	-	-
26	BGU26B	AndT	-	-
31	BGU31	ANDL	UALT	-

Figure 5 Footprint plan view of HNL1 geotechnical units

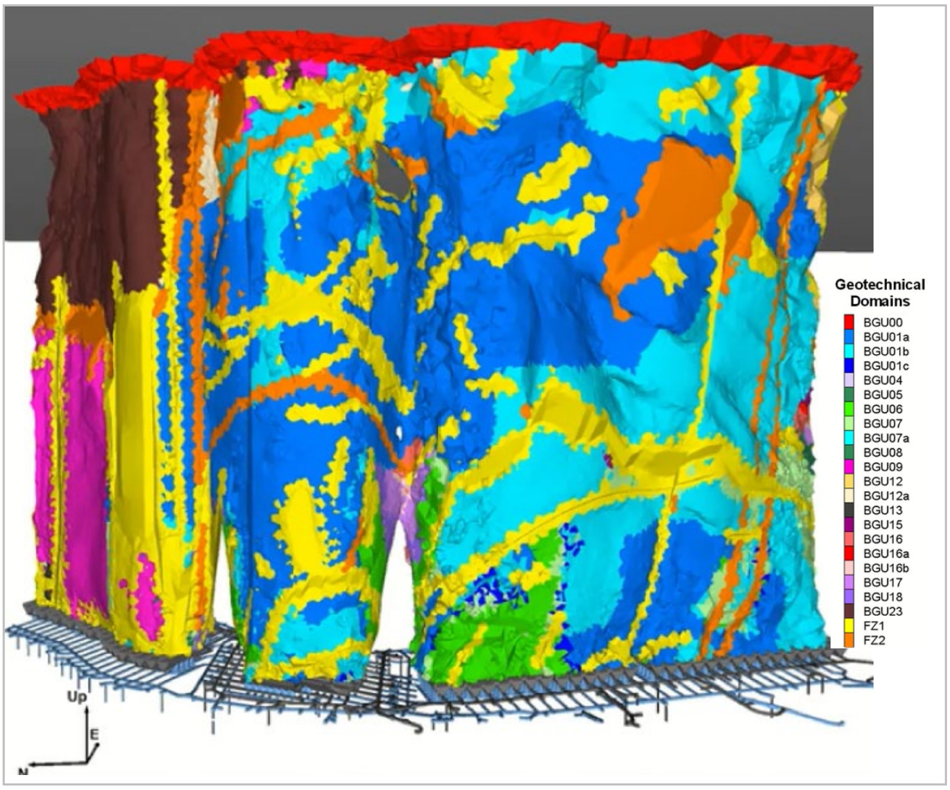

Figure 6 **Cave column view of HNL1 geotechnical units**

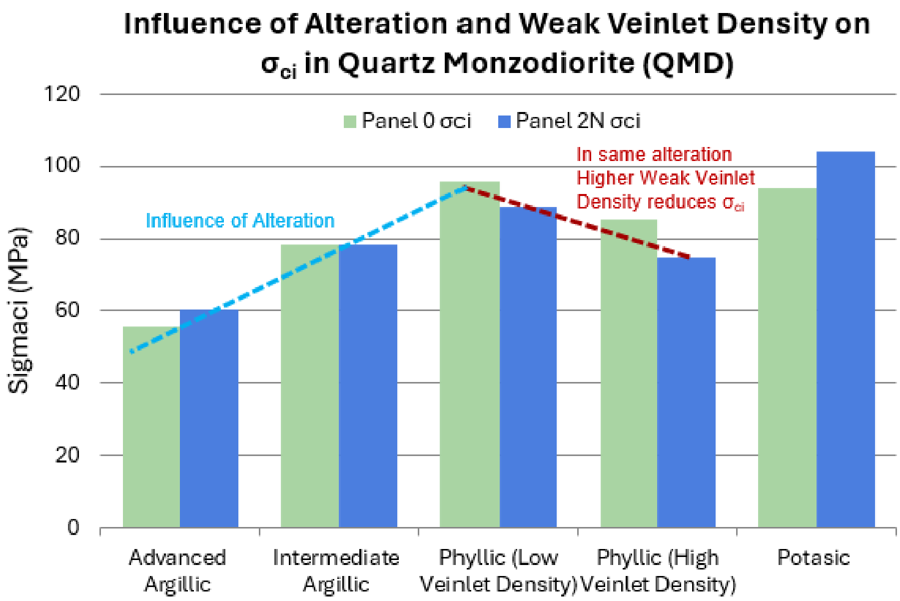

Figure 7 **Influence of alteration and weak veinlet density on intact rock strength in quartz monzodiorite (QMD)**

Table 1 summarises the key geotechnical units relevant to the production footprint and their design significance.

Table 1 Summary of key geotechnical units at Hugo North Lift 1

BGU	Primary lithology	Alteration	Design significance
BGU01a	Biotite granodiorite (BiGd)	Unaltered; low veinlet density	Dominant unit forms the 900 m column overlaying mineralised rock, high strength
BGU01b	Biotite granodiorite (BiGd)	Unaltered; high veinlet density	Present in footprint, weakened by higher weak vein density
BGU06	Quartz monzodiorite (QMD)	PHY; low veinlet density	Moderate strength; widespread footprint
BGU07	Quartz monzodiorite (QMD)	PHY; high veinlet density	Moderate strength; widespread on footprint weakened by higher weak vein density
BGU16	Dacitic–andesitic (IGN)	Mixed AAA + IAA	Moderate strength; east of footprint and materials handling system
BGU18	Andesitic lava (VA)	PTS + PRO + PHY	Moderate strength; east of footprint and materials handling system
BGU01c	BiGd–QMD contact	Lithological contact zone	Heterogeneous; contact zone weakness
FZ1	All lithologies	Weakly cohesive breccia/gouge	GSI ~24; controls footprint stability and cave propagation
FZ2	All lithologies	Moderately cohesive breccia	GSI ~50; controls footprint stability and cave propagation

BiGd: biotite granodiorite; QMD: quartz monzodiorite; IGN: dacitic–andesitic ash-flow tuff; FZ: fault zone; GSI: geological strength index

3 Geotechnical database and data quality

Comprehensive, high-quality geotechnical data with robust spatial coverage across both on- and off-footprint areas and the cave column are fundamental to confident orebody characterisation and block cave design (Laubscher 2000; Brzovic & Villaescusa 2007; van As & Noppé 2024). Brzovic & Villaescusa (2007) established at El Teniente that rock mass disassembly during caving is primarily controlled by the frequency and character of small-scale veins and veinlets rather than large-scale structure alone – a finding that directly motivated the spatially comprehensive veinlet logging program at Hugo North. Incomplete or spatially biased datasets remain one of the primary sources of geotechnical uncertainty in feasibility-stage caving studies (Jakubec & Laubscher 2000).

The HNL1 characterisation program was underpinned by an extensive geotechnical dataset compiled from approximately 400 drillholes (129,140 m total) and 4,300 m of underground tunnel mapping in Panel 0. The focus of drilling was the block cave, encompassing the 500 m cave column and the overlying 800 m of barren rock. Infrastructure locations to the east and west of the block cave were also an area of focus. The spatial distribution of data across the deposit is illustrated in Figure 8. Data collection was phased progressively through the panels as the study advanced.

Panel-specific contributions to geotechnical core logging and, where available, face mapping was as follows:

- Panel 0–2N: ~64,630 m of core logged and 4,300 m of face maps
- Panel 1: ~33,130 m
- Panel 2S: ~31,380 m.

Tunnel mapping in Panel 0 provided the only direct face observation of in situ rock mass conditions and was used to validate drillhole-derived geotechnical rock mass classifications.

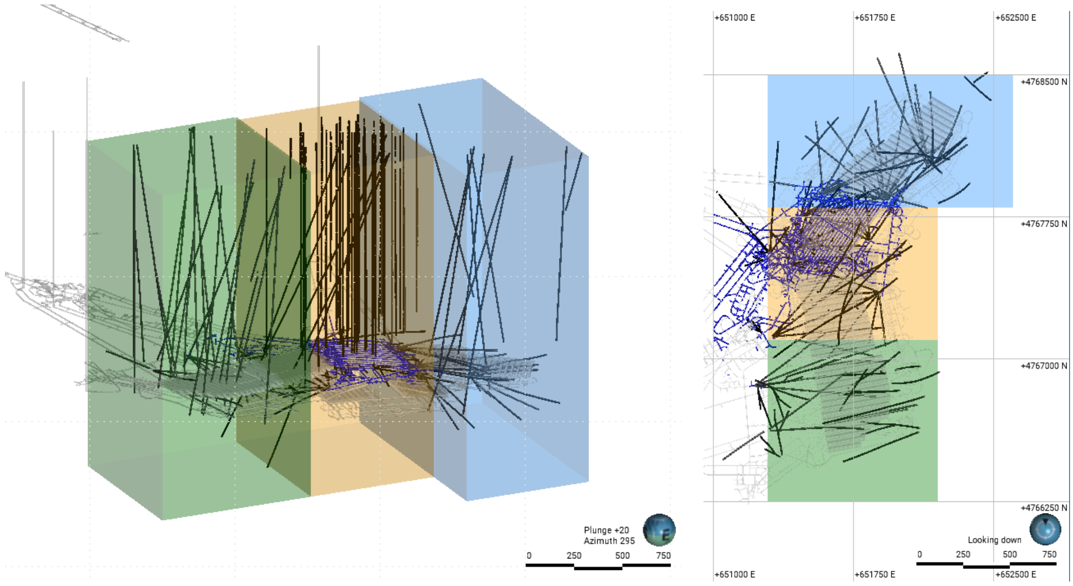

(a) (b)

Figure 8 Drillhole and tunnel mapping distribution – Panel 1 (blue), Panel 0-2N (orange), Panel 2S (green). (a) Isometric view; (b) Plan view

All geotechnical data underwent rigorous validation before use. Internal consistency was confirmed by cross-checks between correlated parameters including rock quality designation (RQD) versus fracture frequency, σci versus alteration index, Bieniawski joint condition versus Barton joint alteration (J_a), and rock mass alteration versus joint wall condition. Figure 9 demonstrates the good-to-fair cross-correlation between the rock mass rating classification systems of RMR_{B89} (Bieniawski 1989) and RMR_{L90} (Laubscher 1990) and the classification systems of $IRMR_{2001}$ (Laubscher & Jakubec 2001) and RMR_{L90} (Laubscher 1990), providing confidence in the reliability of the database across all panels.

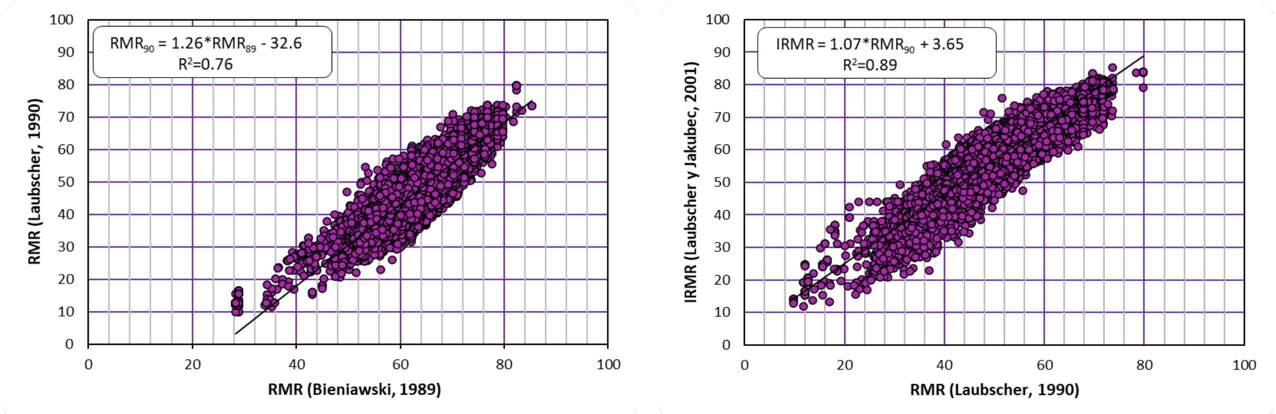

Figure 9 Cross-correlation between rock mass classification systems confirming database reliability. (a) Rock mass rating (RMR) (Bieniawski 1989) versus RMR (Laubscher 1990); (b) In situ rock mass rating (Laubscher & Jakubec 2001) versus RMR (Laubscher 1990)

The HNL1 laboratory testing program comprised 650 uniaxial compressive strength (UCS), 2,062 triaxial compressive strength (TCS) tests, 323 uniaxial tensile strength and 167 block punch tests. The tests were distributed across each of the different planned mining panels. The large volume of testing was driven by the need to capture spatial variability across the 2 km × 500 m footprint (Figure 10) across the multiple alteration and weak veinlet density based geotechnical domains.

All test samples underwent failure mode classification (Russo & Hormazábal 2016) review by the Geotechnical team before use. Type A (matrix failure), Type B (matrix + vein failure) and Type C (multiple veinlet failure) were retained as valid intact rock results. Type D (single veinlet failure) was redirected to the shear strength characterisation program.

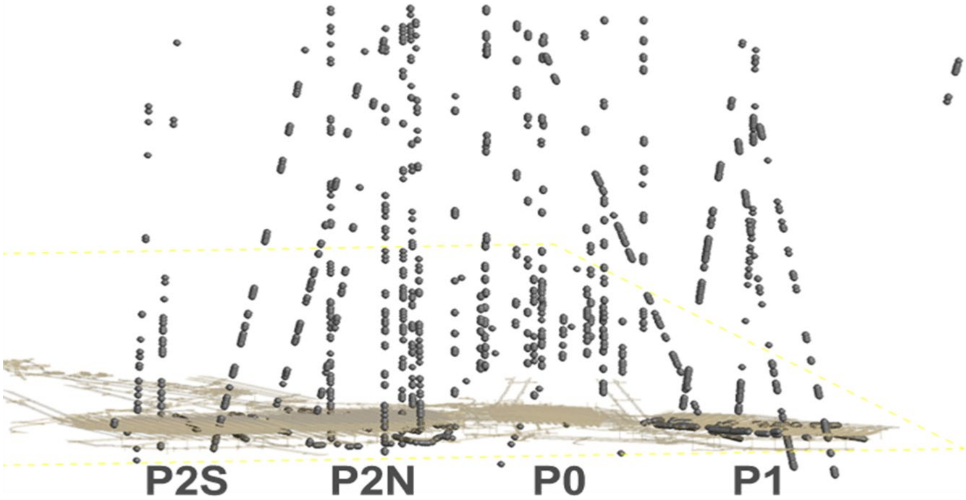

Figure 10 Spatial distribution of Hugo North Lift 1 intact rock samples

4 Rock mass classification

4.1 Rock mass classification results

Rock mass quality was estimated for each BGU using several classification systems: RMR_{B89} (Bieniawski 1989), RMR_{L90} (Laubscher 1990), $IRMR_{2001}$ (Laubscher & Jakubec 2001), Q' (Grimstad & Barton 1993), GSI_{95} (Hoek et al. 1995), GSI_{2013} (Hoek et al. 2013) and $GSI_{R\&H2019}$ (Russo & Hormazábal 2019). The use of multiple systems provides cross-referencing capability and supports numerical modelling input that may require specific classification parameters.

A vertical geotechnical zonation was applied throughout the deposit. From the surface to 50 m surface level the shallow secondary (supergene) zone was identified. This zone is affected by meteoric weathering and oxidation and exhibits significantly lower rock mass quality than the deeper primary zone, which is more competent with sealed unaltered veinlets. The primary zone is subdivided into two zones: the cave column extending to 100 m above the production level and below this, the undercut zone which hosts the production levels and footprint access. The two zones were differentiated because of their different uses. The cave column was delineated for managing subsidence and fragmentation and the undercut zone was delineated for footprint access and footprint infrastructure, including production drives and drawpoints.

A consistent finding across all panels is a slight degradation in rock mass quality in the undercut zone relative to the caving propagation zone above. This reflects the concentration of hypogene alteration at the core of the porphyry system where the orebody and the production level coincide. The typical primary zone rock mass at Hugo North falls in the poor-to-fair range, $GSI_{R\&H2019}$ is 58–65 and RMR_{L90} is 40–50 for the BiGd and QMD units. Within the FZ1 fault zone, $GSI_{R\&H2019}$ is 33 and RMR_{L90} is 22–27. Table 2 presents the consolidated primary zone classification results for the key BGUs across all panels.

Table 2 Weighted average of geotechnical parameters and classification systems of main geotechnical units in Panel 1, Panel 2S and Panel 0-2N in the undercut zone

Panel	GU	RMR_{B89}	$IRMR_{L\&J2001}$	RMR_{L90}	$GSI_{R\&H2019}$	GSI_{1995}	Q'_{2013}
Panel 1	BGU01a	61	51	44	61	56	7.37
	BGU01b	59	47	42	59	54	9.81
	BGU07	61	50	45	61	56	9.95
	BGU16	59	51	43	61	55	5.83
	BGU18	62	54	46	63	57	9.81
	FZ1	42	32	27	41	37	0.99
	FZ2	55	45	41	59	50	5.31
Panel 2S	BGU01a	63	54	47	64	58	9.66
	BGU01b	62	52	46	63	57	11.24
	BGU07	60	49	44	61	55	7.95
	BGU16	59	48	43	60	54	7.12
	BGU18	64	57	50	65	59	10.15
	FZ1	37	29	22	34	32	0.61
	FZ2	53	43	40	58	48	4.60
Panel 0-2N	BGU01a	62	52	44	61	57	10.27
	BGU01b	61	49	41	58	56	10.87
	BGU07	62	52	43	61	58	11.01
	BGU16	62	54	43	60	57	8.79
	BGU18	63	54	44	61	58	9.39
	FZ1	38	31	22	33	33	0.68
	FZ2	55	50	33	50	50	5.04

Values represent weighted averages from geotechnical drillhole composite databases. Q′ values are calculated without the Jw/SRF water/stress correction.

5 Intact rock strength characterisation

5.1 Sampling program and failure mode classification

A total of 2,712 UCS and TCS tests were completed across the whole mining footprint, representing one of the largest intact rock testing campaigns undertaken for a block cave pre-feasibility and feasibility program. Table 3 provides the break down of the number of tests per panel and test type. The higher TCS: UCS ratio reflects the importance of accurately constraining the curvature of the Hoek–Brown failure envelope (m_i parameter) rather than relying on UCS alone.

Table 3 Number of tests within the actual cave boundary for each mining panel

Triaxial test				Unconfined compression test				Triaxial and unconfined compression test
Panel 1	Panel 0	Panel 2N	Panel 2S	Panel 1	Panel 0	Panel 2N	Panel 2S	Infrastructure
237	490	541	80	122	113	210	41	878

A critical step in intact rock data processing for hydrothermally altered porphyry rocks is the classification of sample failure modes following the methodology of Russo & Hormazábal (2016) which has been adopted at Oyu Tolgoi. This approach explicitly accounts for the influence of the stockwork of mineralised veins and veinlets in controlling the failure behaviour of laboratory test samples and classifies them as follows:

- Type A (failure through intact rock matrix): valid for intact rock property estimation
- Type B (failure through combined rock matrix and veins): valid for intact rock strength estimation
- Type C (failure along multiple veinlets): valid for intact rock strength estimation
- Type D (failure along a single veinlet): excluded from intact rock analysis; used for veinlet shear strength. Approximately 30–35% of all tests are classified as Type D failures.

This classification framework enables filtering of non-representative failure modes while accounting for the role of microdefects.

Estimation of the intact strength properties for the different BGUs followed the standardised Hoek–Brown criterion (Hoek et al. 2002; Hoek & Brown 2019). The Levenberg–Marquardt regression in RocData v5.0 (Rocscience 2016) was used to fit the σci and m*i* parameters, targeting σci values consistent with the full range of valid UCS tests. Results failing below the Mogi line (the brittle-ductile transition; Mogi 1966) were also excluded as the Hoek–Brown criterion is not considered valid in the ductile regime. Following the Hoek & Brown (2019) recommendations, tensile strength test values were not used; the Hoek & Martin (2014) equation was used to estimate the tensile rock mass strength.

5.2 Key results and insights

The intact rock property results are broadly consistent across panels for shared BGUs, confirming the reliability of the BGU framework and dataset. The dominant BiGd and QMD BGUs together cover much of the production footprint and show the clear vein density control on strength. Table 4 provides a cross-panel synthesis of the key Hoek–Brown parameters.

Table 4 Hoek–Brown intact rock parameters for key geotechnical units

BGU	Typical lithology/alteration/vein density	σci (MPa)	m_i	UCS_{50} (MPa)	Young's modulus (GPa)	Poisson's ratio
BGU01a	BiGd, Unaltered, Low Weak Veinlet density	94–131	10–20	91–113	41–50	0.15–0.22
BGU01b	BiGd, Unaltered, High Weak Veinlet Density	61–74	14–22	61–86	32–46	0.16–0.31
BGU06	QMD, PHY, Low vein	76–96	17–19	70–80	47–50	0.18–0.23
BGU07	QMD, PHY, High Weak Veinlet	68–85	12–28	61–73	27–51	0.18–0.28

BGU	Typical lithology/alteration/vein density	σci (MPa)	m_i	UCS_{50} (MPa)	Young's modulus (GPa)	Poisson's ratio
BGU08	QMD, PTS + Unaltered	72–104	14–24	57–88	27–55	0.19–0.27
BGU16	IGN, dacitic–andesitic tuff, AAA + IAA	62–83	10–13	74–83	44–68	0.21–0.24
BGU18	VA, andesitic lava, PRO + PTS	79–111	10–12	88–112	51–65	0.16–0.27

σci: uniaxial compressive strength of intact rock; m_i: Hoek–Brown intact parameter; UCS_{50}: mean UCS (50 mm diameter equivalent).
Ranges represent inter-panel variability.

Several geotechnical insights emerge from this dataset that are particularly relevant for caving design:

- Weak vein density is the dominant control on intact rock strength variability within the BiGd and QMD BGUs, more so than alteration type. GU01b and GU07 (high vein density variants) have σci values 30–40% lower than their low weak veinlet density counterparts (GU01a and GU06, respectively).
- The m_i parameter exhibits high variability within individual BGUs (range ~8–28 across the QMD BGUs), reflecting the mixed influence of alteration, veinlet geometry, and mineralogy on post-peak brittleness. This variability has direct implications for fragmentation modelling, which is sensitive to m_i.
- Potassic alteration (e.g. GU08) tends to preserve or slightly enhance intact strength relative to the unaltered equivalent, while advanced argillic and phyllic alteration progressively reduce it. Propylitic alteration has an intermediate effect.
- The overall intact rock strength range for the footprint (UCS_{50} typically 60–115 MPa for the dominant BiGd and QMD BGUs) places the Hugo North orebody in the moderate strength category for a caving system. Combined with the high stress conditions at depth, this results in a challenging environment for maintaining the accessibility and operational reliability of undercut and extraction level excavations, as well as production drawpoints.
- Tensile strength was estimated using the Hoek & Martin (2014) relationship rather than direct Brazilian test results, consistent with the Hoek & Brown (2019) guidance, generating conservative tensile strength values (typically −4 to −8 MPa for the dominant units).
- Attaining good quality and quantity of data is a critical consideration in the planning of the rock strength testing program. Due to the complex nature of porphyry deposits, approximately 65–70% of all tests returned valid test results that were suitable for deriving intact rock strength parameters.

6 Fault characterisation

6.1 Classification framework

Major structures at Hugo North were classified using a two-tier framework based on fault thickness and infill material characteristics (Table 5). Fault core thickness provides a distinction between fault planes and fault zones. Fault planes are defined by core thicknesses <1 m and typically behave as discrete discontinuities, whereas thicker structures (≥1 m) form fault zones that exhibit rock mass behaviour with bulk geomechanical properties.

Both fault classes are considered to influence stability and caveability at different scales. In addition, thicker faults may contain internal zones of reduced thickness that locally exhibit discontinuity-controlled behaviour.

Table 5 Classification framework for major structures at Hugo North

Fault type	Fault thickness	Description	Characterisation approach	Block model treatment
Fault plane	<1 m	Very weak plane (gouge-filled)	Cohesion: Peak 75 kPa, Residual 0 kPa Friction Angle: Peak 25˚, Residual 20˚ Barton–Bandis shear envelope	• Modelled as explicit structural planes • Excluded from 5 × 5 m block model • Applied directly in numerical analyses • Incorporated into mine planning and design
Fault zone 1 (FZ1)	≥1 m	Weakly cohesive breccia/fault zone with gouge	Rock mass properties (GSI ~24–33)	• Volume-weighted downgrade in block model • Applied directly in numerical analyses • Incorporated into mine planning and design
Fault zone 2 (FZ2)	≥1 m	Moderately cohesive breccia	Rock mass properties (GSI ~50)	• Volume-weighted downgrade in block model • Applied directly in numerical analysis • Incorporated into mine planning and design

The distribution of fault core thickness derived from drillcore logging at Hugo North (Figure 11) supports the application of a 1 m threshold for geomechanical classification. Two distinct populations are observed: thin fault cores (<1 m), interpreted as fault planes, and thicker fault cores (≥1 m), interpreted as fault zones.

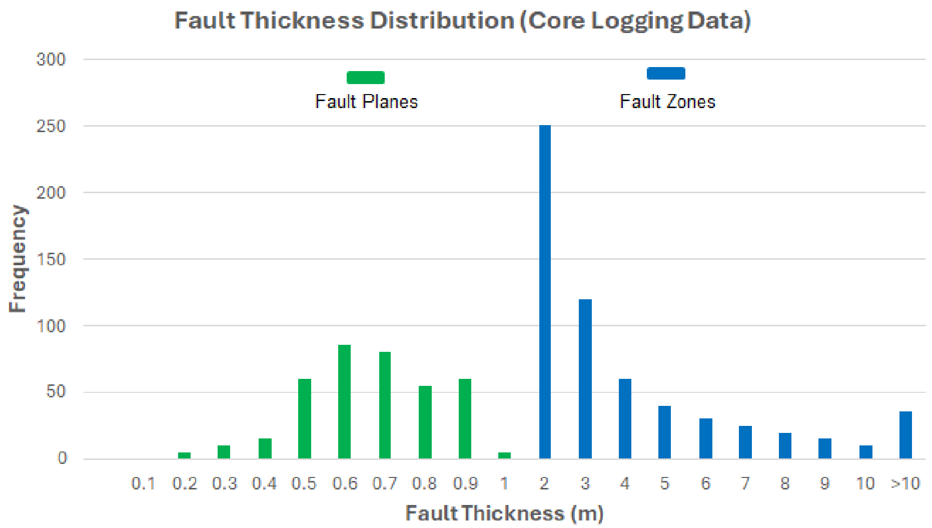

Figure 11 Histograms of thickness of faults identified from core logging. Fault planes <1 m, fault zones (≥1 m)

6.2 Fault zone geotechnical properties

Fault zones (FZ1 and FZ2, core ≥1 m) were characterised as degraded rock mass zones (Figures 12 and 13, respectively). The characterisation of fault zones combined drillcore logging of fault intercepts; structural mapping from Panel 0 tunnel exposures; and statistical analysis of rock mass classification parameters within fault-coded drillhole intervals. Table 6 summarises the geotechnical parameters for FZ1 and FZ2.

Figure 12 Weakly cohesive fault zone 1 (FZ1)

Figure 13 Moderately cohesive fault zone 2 (FZ2): cataclasite-dominated breccia

Table 6 Rock mass classification of faults

Fault zone	RQD	RMR_{B89}	$IRMR_{L\&J2001}$	RMR_{L90}	$GSI_{R\&H2019}$	GSI_{95}
FZ1	12	37–42	29–32	22–27	24–33	24–33
FZ2	50	53	43–50	33–41	48–50	48–50

FZ1: weakly cohesive – gouge, rubble, non-cohesive breccia; FZ2: moderately cohesive – cataclasite, cemented breccia; RQD: rock quality designation; RMR: rock mass rating; IRMR: in situ rock mass rating; GSI: geological strength index

The FZ1 classification ($GSI_{R\&H2019}$ ≈24–33, RMR_{L90} ≈22–27) places these zones in the 'very poor' rock mass category, consistent with gouge-dominated fault cores. The FZ2 classification ($GSI_{R\&H2019}$ ≈48–50,

RMR_{L90} ≈33–41) falls in the 'poor-to-fair' category. Both are significantly lower quality than the surrounding footprint rock mass ($GSI_{R\&H2019}$ 55–65 and RMR_{L90} ≈40–50), and their spatial distribution therefore exerts a disproportionate influence on on-/off-footprint infrastructure stability, undercut sequence, cave propagation and surface subsidence extents.

6.3 Fault plane shear strength

Fault plane shear strength was characterised using triaxial test results where failure occurred along a pre-existing veinlet or fault plane (Type D failures). The Goodman (1989) stress transformation was applied to extract normal stress (σ_n) and shear stress (τ) acting on the discontinuity from the confining stress (σ_3) and peak axial stress (σ_1) at failure. Barton–Bandis shear envelopes (Barton & Bandis 1980) were then fitted, yielding joint roughness coefficient (JRC) and joint compressive strength (JCS) parameters for each fault plane category.

Scale effects – the progressive reduction in apparent roughness and cohesion with increasing trace length – were explicitly accounted for by applying the Barton–Bandis JCS and JRC scaling relations (Bandis et al. 1981; Barton & Choubey 1977). Three scales were considered: sample scale (5–10 cm), drift scale (5–10 m) and large scale (50–100 m), corresponding to the key design dimensions for brow stability, pillar analysis and footprint-scale cave propagation, respectively. Bandis et al. (1981) demonstrated empirically that scale effects are most pronounced for rough, undulating joints – the predominant joint type in the phyllic alteration zones at Hugo North – and negligible for planar surfaces. This distinction directly informed the decision to apply separate scale corrections for the phyllic and non-phyllic alteration groups in this study.

Alteration type of the vein or fault wall proved to be the most consistent grouping criterion in the absence of reliable mineral fill descriptions for all Type D failures. Two strength groups were defined: Group 1 (stronger, associated with argillic, unaltered and propylitic wall alteration) and Group 2 (weaker, associated with phyllic wall alteration). The phyllic group consistently showed lower JCS and JRC values, reflecting the clay-rich fault gouge commonly associated with phyllic alteration in porphyry systems.

7 3D geotechnical block model

7.1 Block model architecture and estimation strategy

A 3D geotechnical block model was developed in Vulcan at 5 × 5 × 5 m block resolution to cover the full Hugo North Lift 1 footprint and cave column. This resolution was selected to balance computational tractability with the need to resolve geotechnical variability at a scale relevant to drawpoint spacing and production scheduling.

The model integrates:

- 3D geological wireframes: lithology, alteration type, weak veinlet density and major fault structures – used to assign geotechnical unit codes to each block.
- Basic geotechnical parameters estimated by geostatistical interpolation: RQD, joint spacing, intact rock strength, rock block strength, Bieniawski joint condition, Laubscher joint condition, Laubscher & Jakubec joint condition, cemented vein frequency, joint roughness, joint alteration and joint set number.
- Calculated rock mass classification outputs: Bieniawski RMR_{B89}, Laubscher RMR_{L90}, Laubscher & Jakubec $IRMR_{L\&J2001}$, Barton Q' and GSI – derived by scripted calculation from the estimated basic parameters in each block.

Two geostatistical estimation methods were employed, selected per BGU based on data density and variogram behaviour. Ordinary kriging (OK) was applied as the primary method where sufficient data and interpretable variograms existed, using passes at the variogram range, twice the range, and extended passes (up to 5,000 m in the final pass) to ensure full model coverage. This approach follows the precedent established by Stavropoulou et al. (2007), who demonstrated that OK provides reliable three-dimensional representation of rock mass properties and that cross-validation of spatial continuity confirms estimation fidelity at the block scale. The inverse distance method was applied to BGUs with sparse data or variograms exhibiting pure nugget behaviour, where kriging would produce unreliable estimates.

As QA/QC, the nearest neighbour (NN) method was applied to evaluate the percentage variation between estimated input parameters (RQD, fracture frequency, spacing, intact rock strength, joint roughness and joint infill and the corresponding calculated statistics derived from sample data. This assessment was used to confirm that mean values estimated by BGU are consistent with the underlying input data. Figure 14 provides a distribution of RMR_{L90} and $GSI_{R\&H2019}$ on the footprint of elevation of HNL1.

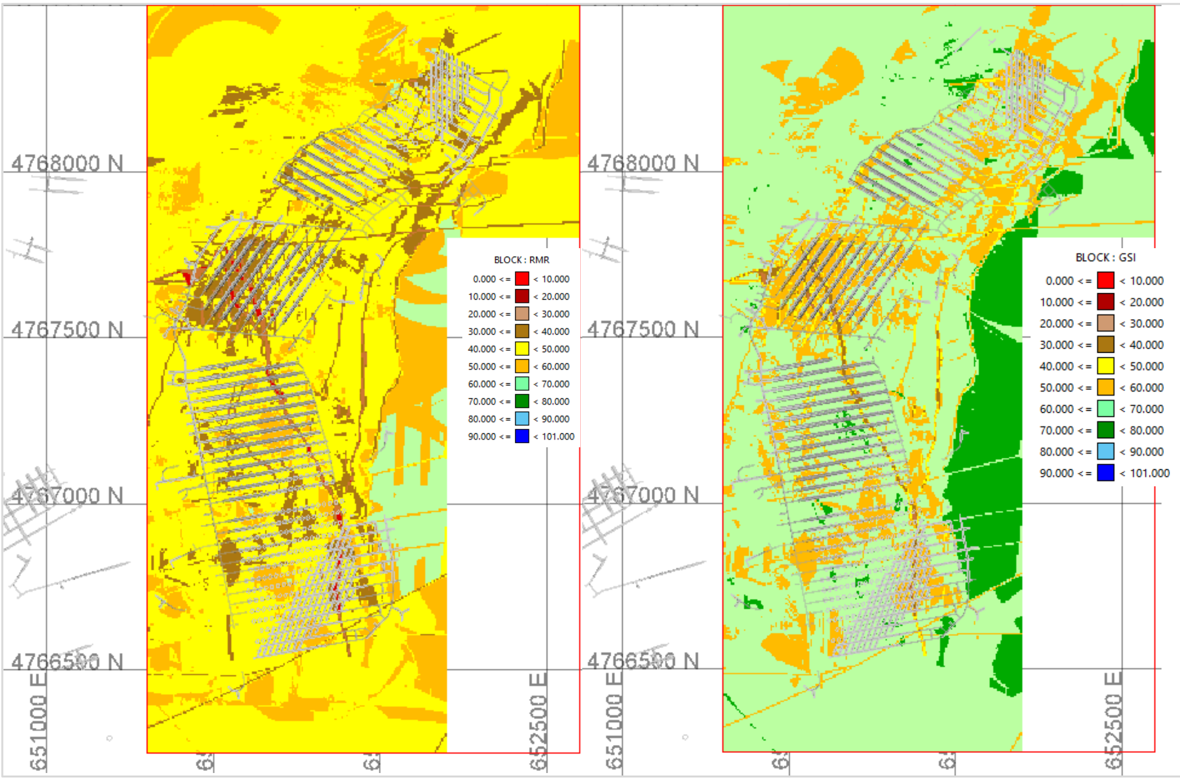

Figure 14 RMR_{L90} and $GSI_{R\&H2019}$ plots of HNL1 footprint in block model

7.2 Structural model integration and fault downgrading

A fundamental challenge in geotechnical block modelling of structurally complex rock masses is the underrepresentation of major fault zones. Because fault zones typically constitute a small fraction of any individual block volume – often less than 20% even where the structure intersects the block – a standard estimation approach assigns the block a quality dominated by the surrounding rock mass, masking the significant local degradation caused by the fault. This produces a systematically optimistic block model that does not reflect the conditions observed in drillcore or tunnel mapping.

To address this, the 3D structural model was explicitly flagged into the block model. For every block intersected by a fault zone wireframe, a volume-weighted downgrading algorithm was applied: each geotechnical parameter was recalculated as a weighted average of the rock mass parameter value and the fault zone parameter value, proportional to the percentage of the block occupied by the fault. This approach was applied only to FZ1 and FZ2 (thickness ≥1 m); fault planes were treated as discrete structures for numerical modelling rather than volumetric block model elements.

The downgrading produced a model that better reflected the observed rock mass conditions in fault-proximal blocks. Where major FZ1 structures cross the production footprint, the block model now shows bands of GSI 24–35 embedded within the background GSI 50–60 rock mass, consistent with the observations from Panel 0 tunnel mapping and drillcore. In addition, the fault volume percentage was stored as a separate model attribute in each block, enabling downstream numerical modellers to perform fault thickness sensitivity studies at higher spatial resolution without rebuilding the block model.

The block model has been applied directly to caveability assessments (based on MRMR, following Laubscher 2000), hydraulic radius calculations for footprint stability, fragmentation predictions, subsidence modelling, and production panel sequencing. The structural integration step was identified as having the most material impact on footprint stability outputs, particularly where FZ1 fault zones trend subparallel to the undercut front as well as the caveability whereby caving was observed to be largely driven by structure. The importance of rigorous characterisation inputs to these assessments is underscored by Bewick et al. (2022), who identified poor rock mass characterisation – particularly failure to resolve the key elements controlling rock mass disassembly – as a primary driver of revenue recovery shortfalls in historical block cave operations.

7.3 Reducing geotechnical uncertainty: risk ranging application of block model

Two Hoek–Brown rock mass strength cases were developed from the 3D block model to define a range of possible ground conditions, enabling assessment of footprint reliability, caveability and subsidence, and reducing geotechnical uncertainty to support design and mitigation strategies. A low-range case is based on GSI_{95}, representing a reduced-strength scenario and a central-range case is based on $GSI_{R\&H2019}$, representing a moderate strength condition.

Figure 15 presents a comparison of global rock mass strength for the two cases. Weak zones (blue) align with mapped structural features and exhibit strength characteristics consistent with the adopted fault classification.

As part of the design process, stability and caveability modelling results from both cases were used to identify problem areas and inform mitigation strategies. These rock mass models have been continuously calibrated and updated using observed rock mass response during caving, supplemented by face mapping, drilling data and ongoing structural model updates.

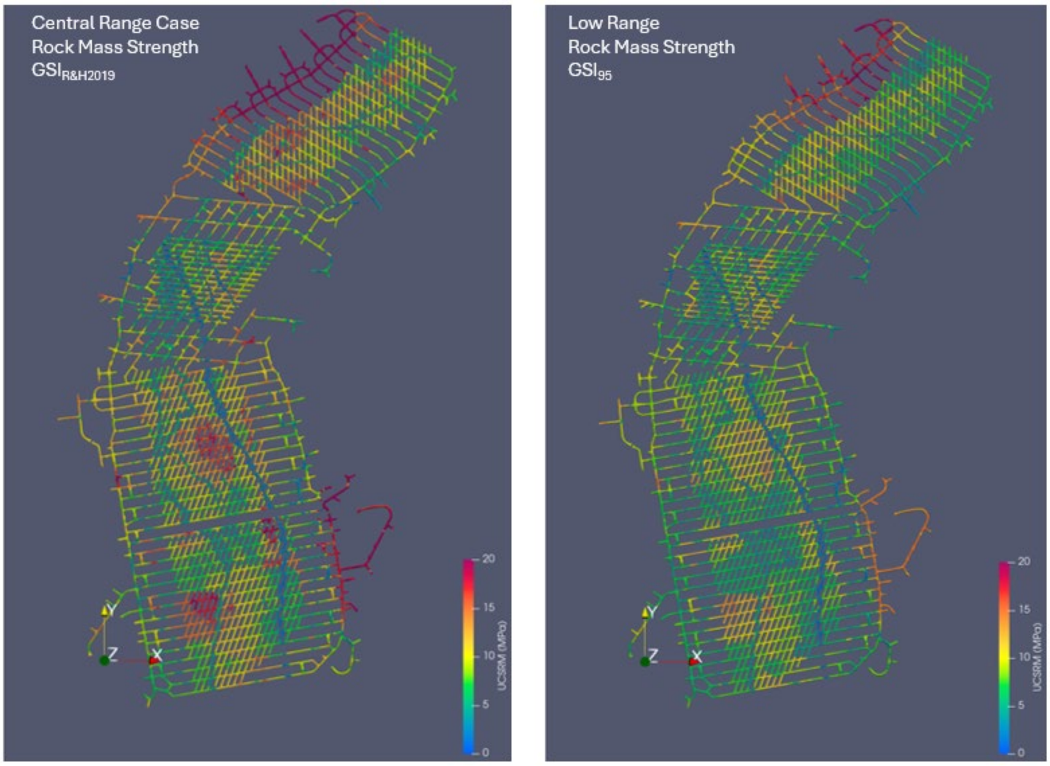

Figure 15 Comparison of central range ($GSI_{R\&H2019}$) and low range (GSI_{95}) rock mass strength cases for risk ranging

8 Conclusions and lessons learnt

A comprehensive geotechnical characterisation program has been executed for Hugo North Lift 1 – one of the largest and deepest block caves currently in production. Characterisation was built on approximately 129,140 m of drillcore and 4,300 m of tunnel face mapping collected over 4 years and culminated in an integrated 3D geotechnical block model covering all four mining blocks.

A key objective of this work was to reduce geotechnical uncertainty through the development of multiple Hoek–Brown rock mass strength cases, defining a risk envelope for caveability, footprint reliability and subsidence response. This framework provided a robust basis for design evaluation and mitigation planning.

The following conclusions and lessons learnt are presented for the benefit of the broader block caving community:

- Geotechnical unit definition in porphyry systems must go beyond lithology and alteration. The addition of weak veinlet density as a discriminating parameter was essential at Hugo North. The dominant BiGd and QMD BGUs showed 30–40% reductions in σci when crossing the 15 veinlets per metre threshold, with corresponding reductions in block model quality sufficient to alter caveability and fragmentation predictions. In complex porphyry systems, domain boundaries defined on lithology and alteration alone will produce misleadingly uniform geotechnical characterisation.
- Failure mode classification is non-negotiable in hydrothermally altered rock masses. Standard laboratory practice produces biased intact rock parameters in vein-rich or altered samples. The application of the Russo & Hormazábal (2016) failure mode classification framework to the 2,712-test dataset at Hugo North filtered out Type C failures that would otherwise have artificially elevated σci estimates. The Type D failures were not wasted data – they were repurposed for shear strength characterisation of cemented veinlets, demonstrating the value of designing a testing program that anticipates failure mode outcomes. The complexity of the orebody will determine the geotechnical sampling volumes – often, minimum ISRM (International Society for Rock Mechanics) specifications are inadequate when dealing with multi-domain, complex orebodies. Extensive sampling was therefore completed across the domains.
- Multi-scale shear strength characterisation is necessary for fault and veinlet-rich porphyry caves. The Barton–Bandis scale-effect corrections applied at sample, drift and large scale produced meaningfully different shear strength envelopes for the same geological feature. Using sample-scale parameters at the footprint scale would overestimate joint and fault strength. Separate characterisation of the phyllic versus non-phyllic alteration groups was also shown to be significant, with phyllic-associated features consistently yielding lower strength.
- Explicit structural model integration is essential for realistic block model outputs. Extensive characterisation of faulting was undertaken and incorporated; however, the characterisation of faults along their strike remains complex and is the focus of ongoing work. The initial block model without structural downgrading overestimated rock mass quality in fault-proximal zones. The volume-weighted downgrading approach described in Section 6 produced a model that is demonstrably more consistent with direct observations from drilling and mapping. The decision to store fault volume percentage as a block model attribute added significant downstream value for numerical modelling teams conducting sensitivity analyses without requiring block model rebuilding.
- The characterisation workflow and integrated block model described in this paper have reduced geotechnical uncertainty across all design phases of Hugo North Lift 1. The methodology is considered transferable to other large-footprint porphyry block caves facing similar challenges of hydrothermal alteration variability, veinlet stockwork complexity and structurally controlled rock mass degradation.

Acknowledgement

This paper is a result of several years of hard work put in by many different teams at Oyu Tolgoi namely the resources & systems team, UG geology & geotechnical services team, logistics team and Rio Tinto T&SMP geosciences team. A special thank you to the Management Teams of Oyu Tolgoi and Rio Tinto for permission to publish this paper.

References

Bandis, S, Lumsden, A C & Barton, N 1981, 'Experimental studies of scale effects on the shear behaviour of rock joints', *International Journal of Rock Mechanics and Mining Sciences & Geomechanics Abstracts*, vol. 18, no. 1, pp. 1–21.

Barton, N & Bandis, S 1980, 'Some effects of scale on the shear strength of joints', *International Journal of Rock Mechanics, Mining Sciences and Geomechanical Abstracts*, vol. 17, pp. 69–73.

Barton, N & Choubey, V 1977, 'The shear strength of rock joints in theory and practice', *Rock Mechanics*, vol. 10, pp. 1–54.

Bewick, R, Brzovic, A, Rogers, S, Griffiths, C & Otto, SA 2022, 'Benchmarking framework for porphyry copper-gold rock masses for caveability and fragmentation decision-making', in Y Potvin (ed.), *Caving 2022: Proceedings of the Fifth International Conference on Block and Sublevel Caving*, Australian Centre for Geomechanics, Perth, pp. 1303–1318, https://doi.org/10.36487/ACG_repo/2205_91

Bieniawski, ZT 1989, *Engineering Rock Mass Classifications: A Complete Manual for Engineers and Geologists in Mining, Civil, And Petroleum Engineering*, Wiley-Interscience Publication - John Wiley & Sons, New York.

Brzovic, A & Villaescusa, E 2007, 'Rock mass characterization and assessment of block-forming geological discontinuities during caving of primary copper ore at the El Teniente mine, Chile', *International Journal of Rock Mechanics and Mining Sciences*, vol. 44, no. 4, pp. 565–583.

Day, JM, Diederichs, MS & Hutchinson, DJ 2019, 'Composite geological strength index approach with application to hydrothermal vein networks and intact bridges within shear zones', *Engineering Geology*, vol. 261, 105228.

Goodman, RE 1989, *Introduction to Rock Mechanics*, 2nd edn, John Wiley & Sons, New York.

Grimstad, E & Barton, N 1993, 'Updating of the Q-System for NMT', in R Kompen, OA Opsahl & KR Berg (eds), *Proceedings of the International Symposium on Sprayed Concrete*, Norwegian Concrete Association, Fagernes, pp. 46–66.

Hoek, E, Kaiser, P K & Bawden, W F 1995, *Support of Underground Excavations in Hard Rock*, A.A. Balkema Publishers, Rotterdam.

Hoek, E, Carranza-Torres, C & Corkum, B 2002, 'Hoek-Brown failure criterion – 2002 Edition', in *Proceedings of NARMS-TAC 2002: Mining Innovation and Technology (pp. 267-273),* University of Toronto, Toronto, pp. 267–273.

Hoek, E, Carter, T G & Diederichs, M S 2013, 'Quantification of the geological strength index chart', *Proceedings of the 47th US Rock Mechanics/Geomechanics Symposium 2013*, vol. 13-672, no. 3, pp. 1757–1764.

Hoek, E & Martin, C 2014, 'Fracture initiation and propagation in intact rock–a review', *Journal of Rock Mechanics and Geotechnical Engineering*, vol. 6, no. 4, pp. 287–300.

Hoek, E & Brown, ET 2019, 'The Hoek–Brown failure criterion and GSI – 2018 edition', *Journal of Rock Mechanics and Geotechnical Engineering*, vol. 11, pp. 445–463.

Jakubec, J & Laubscher, DH 2000, 'The MRMR rock mass rating classification system in mining practice', *Proceedings of MASSMIN 2000*, Australasian Institute of Mining and Metallurgy, Melbourne.

Laubscher, D 1990, 'Geomechanics classification system for the rating of rock mass in mine design', *Journal of the South African Institute of Mining and Metallurgy*, vol. 90, no. 10, pp. 257–273.

Laubscher, DH 2000, *Block Caving Manual*, prepared for the International Caving Study, Julius Kruttschnitt Mineral Research Centre, Brisbane.

Laubscher, D & Jakubec, J 2001, 'The MRMR Rock Mass Classification for Jointed Rock Masses', in W Hustrulid & R Bullock (eds), *Underground Mining Methods*, Society for Mining, Metallurgy, and Exploration, Inc. (SME)., Littleton, pp. 475–481.

Mogi, K 1966, 'Pressure Dependence of Rock Strength and Transition from Brittle Fracture to Ductile Flow', *Earthquake Research Institute University of Tokyo*, vol. 44, pp. 215–343.

Rocscience 2016, *RocData*, computer software, Vancouver, https://www.rocscience.com/support/rocdata/

Russo, A & Hormazábal, E 2016, 'A methodology to select valid results from lab tests to estimate properties of intact rock with microdefects', *American Rock Mechanics Association,* Alexandria.

Russo, A & Hormazábal, E 2019, 'Correlations between Various Rock Mass Classifications Systems, Including Laubscher (MRMR), Bieniawski (RMR), Barton (Q)and Hoek and Marinos (GSI) Systems', in *XVI Panamerican Conference on Soil Mechanics and Geotechnical Engineering*, pp. 2806–2815.

Russo, A, Montiel, E & Hormazabal, E 2022, 'Impact of the typical errors in geotechnical core logging for geomechanical design in large caving mines', in Y Potvin (ed.), *Caving 2022: Proceedings of the Fifth International Conference on Block and Sublevel Caving*, Australian Centre for Geomechanics, Perth, pp. 1319–1334, https://doi.org/10.36487/ACG_repo/2205_92

Stavropoulou, M, Exadaktylos, G & Saratsis, G 2007, 'A combined three-dimensional geological-geostatistical-numerical model of underground excavations in rock', *Rock Mechanics and Rock Engineering*, vol. 40, no. 3, pp. 213–243.

Turichshev, A & Hadjigeorgiou, J 2016, 'Triaxial compression experiments on intact veined rock', *Rock Mechanics and Rock Engineering*, vol. 49, no. 2, pp. 445–458.

van As, A & Noppe, M 2024, 'Sufficient geotechnical data for reliable mine design during mining studies', in D Johansson & H Schunnesson (eds), *MassMin 2024: Proceedings of the International Conference & Exhibition on Mass Mining*, Luleå University of Technology, Luleå, pp. 194–207, https://doi.org/10.36487/ACG_repo/2435_B-01